Design And Output Power Evaluation for A Novel Hybrid Wave-Wind Energy Converter

Sadegh Khaleghi, Tek Tjing Lie* and Craig Baguley
Department of Electrical and Electronic Engineering,
Auckland University of Technology,
Auckland 1010, New Zealand
*Correspondence: tek.lie@aut.ac.nz

Abstract: The performance of oscillating water column (OWC) wave energy converters (WEC) is highly affected by airflow rate. In this paper, a novel system is proposed that increases airflow rate and, therefore, output power through the integration of a mechanical structure known as a windcatcher with a conventional OWC. To investigate the hydrodynamic behaviour of the proposed system, a non-linear two-dimensional computational fluid dynamics (CFD) model is employed, along with the Reynolds Averaged Navier-Stokes (RANS) approach. The results of a comparison of the proposed OWC to a conventional type reveal a significant increase in airflow rate through the turbine blades, realizing an increase in converter output power. Moreover, the results show a power generation consistency in the proposed hybrid system, as the amplitude of the oscillatory part of the turbine airflow rate is diminished. Therefore, the proposed OWC converter not only generates significantly more power than a conventional type, it also has smoother power generation performance.

Keywords: Wave Energy Converter; Oscillating Water Column; Windcatcher; CFD; RANS.

1. Introduction

The earth's oceans provide energy in a number of forms that are yet to be fully exploited [1]. One form is wave energy, which on a global scale has a potential capacity estimated to be between 2000 and 4000 TWh per year [2]. Therefore, significant research efforts have been reported on wave energy extracation approaches using wave energy converters (WECs) [3]. This includes the oscillating water column (OWC) type, which has advantages in simplicity [4], and has been the subject of substantial studies and trials [5-8]. An OWC comprises two main components: a main chamber that captures wave energy and

passes it to the air inside the chamber, and a power take-off (PTO) system that coverts pneumatic energy into electricity, or some other practical energy form [6]. A typical arrangement is shown in Figure 1. Trapped air inside the main chamber is pressurized and depressurized by the vertical up-and-down movement of the sea level, resulting in a revolving flow of air through turbines fitted into a small chamber opening at the top [9]. Ref. [10] provides a complete overview of the OWCs and turbines.

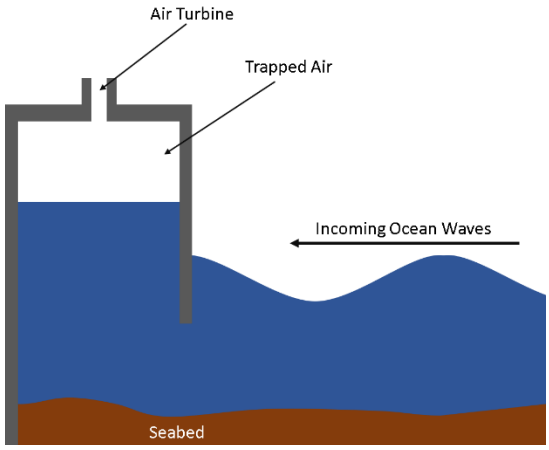

Figure 1. Schematic of a shoreline OWC [11].

Previous efforts to improve the performance of OWCs have mostly focused on hydrodynamic interactions between the device and incident waves [12]-[14]. For example several OWC geometries presented in [12], are compared, including an optimized version that took into account typical wave conditions. In [13] the impact of the length and inclination of the harbour walls when combined with an OWC are studied and a reported 75% increase in the output power to input power ratio is achieved. The findings revealed that an OWC incorporated into a vertical cliff or a harbour is reliant on the region's wave frequency. A model for U-Oscillating Water Column (U-OWC) is implemented in the Natural Ocean Engineering Laboratory (NOEL) by Malara et al. [14]. The model is shown to be capable of explaining water heights in the time domain through experimental verification.

The impact of geometry and the nature of the seabed on OWC performance has been considered more carefully in [15]-[18]. In [15] the influence of seabed inclination on OWC performance is studied for several scenarios to determine the best PTO performance. In [15] a stepped sea bottom is

considered as a dual-mass system to change the water mass in the chamber of OWCs. The numerical modelling approach was verified experimentally. In [16] an investigation is undertaken on the influence of seabed shape on airflow in the turbine, as well as how energy dissipation is affected by the bottom level. A new type of OWC based on employing an innovative dual-chamber is reported in [17] to harvest wave energy in deep water, which falls under a group of studies focussed on modifying the geometry of OWCs to collect more energy. An analytical model is presented to demonstrate that chamber size has a significant impact on effective frequency bandwidth, which increases when the size of a dual-chamber is optimized.

Other work based on investigating the geometry of OWCs to improve performance employ compact fluid dynamic (CFD) simulations in two physical phases. This allows the modelling of complex geometries, and gives insight into the behaviour of working fluids in an OWC chamber and its surroundings in considerable detail.. CFD approaches that solve the Navier-Stokes equations or Reynolds averaged Navier-Stokes (RANS) problems can address intricate nonlinearities. For example, in. [18], a series of two dimensional CFD analyses of a 1:50 scale model are employed to investigate the effect of front and back lip submergence and thickness on OWC performance. These results are experimentally validated, and the major result is that by choosing appropriate values for the submergence ratio of asymmetric lips and the lip thickness, total hydrodynamic efficiency may be greatly enhanced throughout a wide frequency bandwidth. In [19] a three-dimensional CFD analysis is used to examine the hydrodynamics of a circular bottom-sitting OWC system using Navier-Stokes equations, revealing that vortex shedding boosts spatial distinctness inside the OWC cylinder considerably. It was shown that improved spatial non-uniformity significantly affects the precision of experimentally measured values like the extraction efficiency of the OWC and PTO. In [20] an investigation on structural optimization possibilities for further decreasing OWC costs is undertaken. An OWC with an extra vertical channel is analyzed in a three-dimensional field using a one-way coupled hydraulic-structural numerical model. The wave tank is represented by a flow field, and the

OWC structure is described by a solid field. The simulation is done under operational situations and different geometrical modifications to evaluate the energetic performance of the system. They quantified the energetic performance using the mean oscillation amplitude in the chamber of the OWC. It was shown that The reduction in performance for larger ducts is due to increased circulation of airflow within the duct as it becomes larger. In [11] an investigation is undertaken on the power equilibrium of an onshore OWC using a nonlinear two-dimensional RANS-based CFD simulation. It was shown PTO damping and wave height have an important role in vortex production near the top and bottom cylinder mouths throughout the inflow and outflow phases. From the research efforts to characterize and improve the performance of OWCs it is apparent that harnessing the wind to improve the air-flow within OWC chambers has not been reported. Through capturing wind airflows the performance of OWCs can be advanced. WECs make up a small but potentially significant part of the global renewable sources. To compete with offshore wind or solar energy, however, the WEC industry will need to produce viable prototypes that pave the way for up-scaled commercialization. This path requires the use of efficient and reliable numerical modelling approaches to accurately analyze performance metrics during the early design stages [21].

This paper proposes a novel approach that adds a mechanical structure called a windcatcher to the chamber of an OWC to increase the airflow rate and, therefore, the output power that can be generated. Furthermore, a novel turbine placement is introduced. Along with the windcatcher, this allows for the realization of unidirectional airflow with a reduced oscillatory part through the turbine to give smoother output power.

In Section 2 a diagram of the integrated OWC-windcatcher concept is presented along with fundamental theory forming the scientific basis of the approach. In Section 3 system modelling is presented based on finite element method, computational fluid dynamics (CFD), and in Section 4 the simulation set-up is described. In Section 5 resutls are presented showing the benefits and advantages of the proposed approach, and a conclusion is given in Section 6.

2. The OWC-windcatcher Concept

The proposed windcatcher-OWC is designed to improve the speed of the airflow through PTO turbine blades. This is achieved by placing the turbine in a position to use compressed air resulting from free surface water movement inside an OWC chamber as well as wind on top of the ocean. Energy from the wind is captured using a windcatcher, which is integrated into the basic OWC, as illustrated in Figure 2. With the proposed approach, it would be possible to run both unidirectional and bidirectional turbines. The airflow created by the compressed airflow from the OWC primary chamber is controlled by two separate valves.

A windcatcher also referred to as a wind tower, is a classic architectural element designed to facilitate the circulation of air and cooling in buildings. Windcatchers come in a variety of forms and have been used in North Africa and the West Asian regions bordering the Persian Gulf for over 3000 years [22]. Figure 3 shows schematic of a windcatcher. The windcatcher's functionality is powered by two essential forces: buoyancy and exterior wind forces. The buoyancy force is a physical phenomenon generated by temperature changes between the inside and outside of a body. Increasing the number of apertures in a windcatcher improves its effectiveness. Multi-opening windcatchers, on the other hand, are the best choice in locations where there is no significant wind [23].

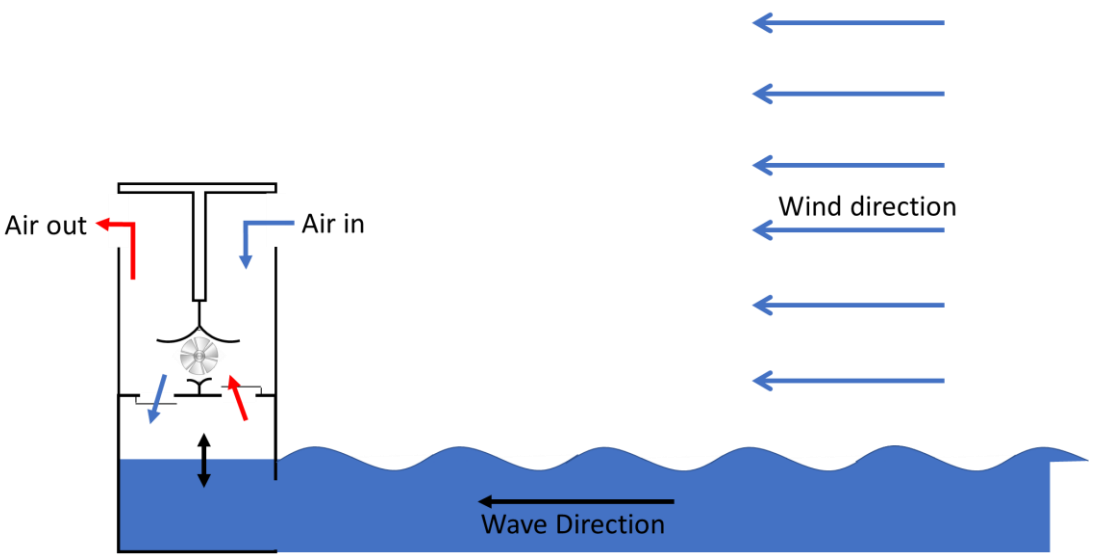

Figure 2. The innovative OWC design combined with the windcatcher concept.

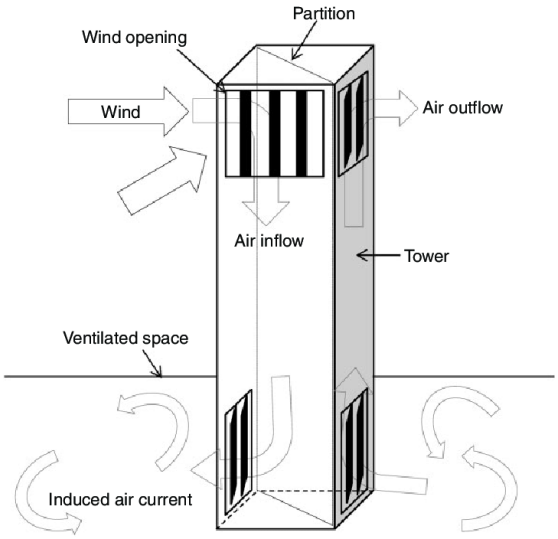

Figure 3. An illustration of windcatcher functionality [23].

Refs. [24-26] have used an orifice or slot to account for the pneumatic damping of PTO and turbine positioning in both experimental and numerical modelling. The orifice is used to account for the turbine pressure drop in both simulations and experiments. Elhanafi et al. [11] also used this method to model the turbine in their research. Furthermore, pressure drops are related to orifice sizes in the flow path (for example, diverse turbine sizes). As a result, the width of the orifice simulates the role of the turbine by causing a pressure drop in the flow. Therefore, the same strategy has been used in this

paper. This work specifies two separate orifices on both sides of the chamber and assigns a different valve to each orifice. When the free surface of the water rises and pressurized air within the chamber forces high-speed air to the turbine blades, one valve opens while the second valve closes. Once the free surface inside the chamber decreases, the second valve opens in the second phase; the air decompression phase begins at this point, and the first valve is closed. During a wave cycle, as the water level in the primary chamber rises, the air is compressed, and the first valve automatically opens, forcing airflow to the turbine blades. During the air decompression phase, the second valve will be opened to fill the chamber with air, while the first valve will be closed. Airflow is captured and sucked into the chamber during this step until the water level returns to normal. Furthermore, the openings of the windcatcher will stay open across the cycle, resulting in a constant airflow rate through the turbine blades. Besides, the hybrid system is designed based on the dominant wind direction. The air inlet and outlet valves of the chamber should be configured to fit the prevailing direction of the wind in the area under study.

The valve opening and closing functions are modelled using a dynamic CFD simulation. The simulation process is divided into two parts. In the first part, the left valve opens, while the right valve closes. The water level within the chamber rises to this point, compressing the air. In the next step, which is air decompression, the left valve opens and the right valve closes as the free surface inside the chamber decreases. Because the opening and closing mechanisms are all dependent on the direction of the airflow rate, each valve opens and closes for half the wave duration. Therefore, the only way to get the air out of the chamber is through the left valve, and the only way to get air in is through the right valve. Finally, the results from steps one and two are combined to show a complete air compression and decompression interval inside the chamber.

Airflow rate ($q(t)$) inside the turbine duct (orifice) of a basic model of an OWC depends mainly on the size of the chamber, size of the orifice and the wave characteristics applied to the inlet boundary. However, for calculating the airflow rate inside the turbine duct of an OWC merged with a

windcatcher, it is necessary to consider other elements like size of the openings, height of the windcatcher and details of the parameters inside the new device which will be explained in the following sections. The total airflow rate inside the proposed OWC comprises the airflow rate provided by OWC and the flow rate of the windcatcher, which can be expressed in (1) as:

$$q(t) = q_{OWC}(t) + q_{windcatcher}(t)\ , \tag{1}$$

where, q(t) is total airflow rates inside the turbine, $q_{OWC}(t)$ is airflow rates comes from the compressed air inside the chamber and $q_{windcatcher}(t)$ shows the airflow rate from the windcatcher. The unit of the mentioned airflow rates are in $m^3\ s^{-1}$.

The airflow rate provided by the OWC and windcatcher is calculated by (2) and (3), respectively:

$$q_{OWC}(t) = V_{freesurface} \times A_{orifice}\ , \tag{2}$$

$$q_{windcatcher}(t) = C_d A_e v_H(t)\sqrt{\Delta C_p}\ , \tag{3}$$

where, $V_{freesurface}$ is the velocity of the water free surface, $A_{orifice}$ is the area of orifice C_d is the coefficient of discharge of the opening in the windcatcher, and v_H (in m s^{-1}) is the velocity at the windcatcher's top wall. Besides C_p is the difference in the pressure coefficient of the air between both the inlet and the outlet of the windcatcher.

Further, the effective area of the opening, indicated by A_e (in m^2), is expressed in (4) as follows:

$$A_e = \frac{A_1 \times A_2}{\sqrt{A_1^2 + A_2^2}}, \tag{4}$$

where, A_1 and A_2 is the area of the inlet and outlet of the windcatcher, respectively.

3. System Modeling

The modelling approach employed includes a series of steps, which are represented in the flowchart in Figure 4 and are discussed in detail in the following sub-sections. The numerical procedure used in this study is given in Section 3.1.

3.1. Numerical Modeling

There are three predominant techniques for numerical modelling of WECs: linear and nonlinear potential flow concept, fully nonlinear potential flow method, and CFD, which solves the Navier–Stokes equations for single phase or two-phase fluids. The most difficult obstacle with the CFD method is precisely resolving the two-phase fluid interface between the water and air within the chamber, especially if the air phase is compressible. The most sophisticated class of numerical models is CFD Navier-Stokes models, which have a high computational cost but can achieve high precision when investigating fully nonlinear systems. The mass conservation equation, also known as the continuity equation, is described in (5) as follows [27]:

$$\frac{\partial \rho}{\partial t} + \nabla.(\rho \vec{v}) = S_m\,, \tag{5}$$

where, ρ is the fluid density, v is velocity vector, and the mass delivered to the continuous phase from the distributed second phase is denoted by the source term S_m.

Furthermore, for a non-accelerating regime referred to as the internal reference frame, conservation of momentum is described in (6) as follows *[27]*:

$$\frac{\partial}{\partial t}(\rho \vec{v}) + \nabla.(\rho \vec{v}\vec{v}) = -\nabla p + \nabla.(\bar{\tau}) + \rho \vec{g} + \vec{F}\,, \tag{6}$$

where, p, $\rho \vec{g}$ and $\vec{F}$ represent the static pressure, gravitational body force and external body forces, caused by interaction with the dispersion phase. $\bar{\tau}$ denotes the stress tensor and it is expressed in (7) as,

$$\begin{cases} \bar{\tau} = \mu[(\nabla \vec{v} + \nabla \vec{v}^T) - VD] \\ VD = \dfrac{2}{3}\nabla.\vec{v}I \end{cases} \tag{7}$$

where, μ is molecular viscosity, I depicts unit tensor, and VD stands for the effect of volume dilation.

ANSYS Fluent is used to create a numerical CFD model to handle the continuity and momentum equations. The air compressibility is only present in large-scale models [12, 28-31]. Besides, the air compressibility is comprehensively analysed by Elhanafi et al. [11]. The result of their study showed that for a scale of 1:50, the results of the compressible and incompressible models are the same. Therefore, the air compressibility has been neglected in the proposed CFD model. RANS and continuity equations are used in simulations to monitor the interaction of water and air, and the *Volume OF Fluid*

procedure is used to determine the motion of the free surface level of water and air. Figure 4 describes the proposed modelling approach used in this study. As seen, the procedure starts with proposing a hybrid wave-wind system and numerical modeling. After that, a suitable turbulence model is chosen and continuity and RANS equations are solved. Consequently, mesh and time-step analysis are conducted, and the obtained result is validated using previous studies. Eventually, the performance indicator of the proposed hybrid system is compared with a baseline (conventional) system.

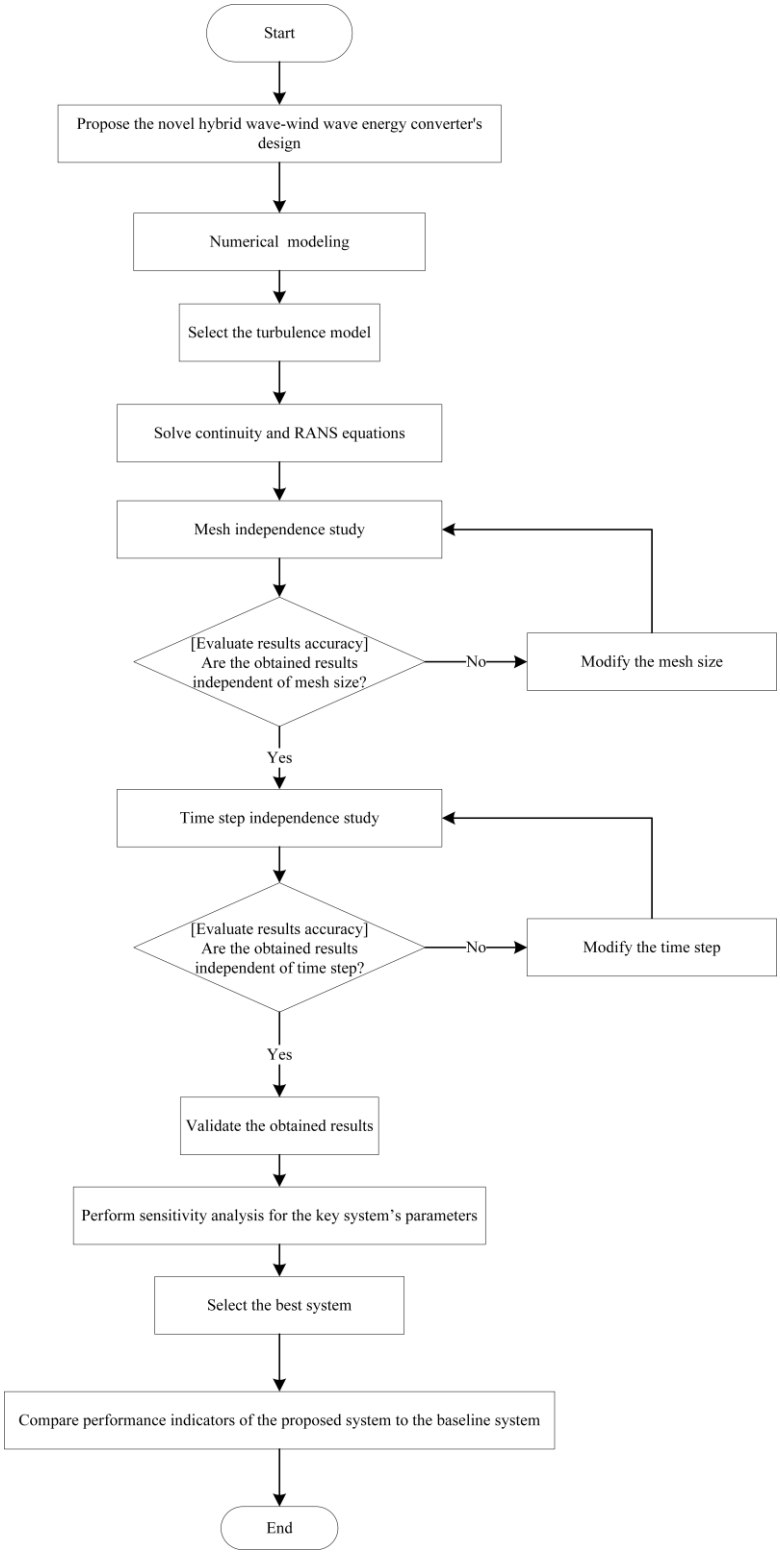

Figure 4. The flowchart of the modelling approach.

3.2. Selection of Turbulence Model

Turbulent flows are distinguished by their constantly changing velocity fields. These variations cause transmitted quantities like velocity, energy, and species concentration to fluctuate as well. Because of their small size and high frequency, these oscillations are too computationally expensive to describe accurately in practical engineering computations [32]. Alternatively, to minimize the resolution of small scales, the instantaneous governing equations can be time-averaged, ensemble-averaged, or otherwise modified, providing a unique set of equations that is computationally less expensive to compute [33]. The new equations contain additional unknown variables that must be computed using turbulence models. Nevertheless, no single turbulence model is universally accepted as superior for all problems. The physics of the flow, the established technique for a specific class of problem, the level of precision required, the available computer resources, and the length of time allotted for simulation will all have an impact on the turbulence model used [34].

The shear-stress transport (SST) $k-\omega$ model is chosen among other available turbulence models for this study. This model is developed by Menter [35] to effectively combine the resilient and highly accurate formulation of the $k-\varepsilon$ model in the near-wall area with the free-stream independence of the $k-\varepsilon$ model in the far field. The equations of transport in the SST $k-\omega$ model are presented in (8) as follows [36],

$$\begin{cases} \dfrac{\partial}{\partial t}(\rho k)+\dfrac{\partial}{\partial x_i}(\rho k u_i)=\dfrac{\partial}{\partial x_j}\left(\Gamma_k \dfrac{\partial k}{\partial x_j}\right)+\tilde{G}_k-Y_k+S_k \\ \dfrac{\partial}{\partial t}(\rho \omega)+\dfrac{\partial}{\partial x_i}(\rho \omega u_i)=\dfrac{\partial}{\partial x_j}\left(\Gamma_\omega \dfrac{\partial \omega}{\partial x_j}\right)+G_\omega-Y_\omega+D_\omega+S_\omega \end{cases}, \tag{8}$$

where, k is turbulence kinetic energy, ω represents specific rate of dissipation $\tilde{G}_k$ denotes the generation of turbulence kinetic energy due to mean velocity gradients. As previously explained, G_ω denotes the formation of ω. Besides, Y_k and Y_ω represent the dissipation of k and ω caused by turbulence. D_ω is the cross-diffusion term. S_k and S_ω are source terms that the user has provided.

Furthermore, Γ_k and Γ_ω indicate the effective diffusivity of k and ω, which is computed as stated in (9),

$$\begin{cases} \Gamma_k = \mu + \dfrac{\mu_t}{\sigma_k} \\ \Gamma_\omega = \mu + \dfrac{\mu_t}{\sigma_\omega} \end{cases}, \tag{9}$$

where, σ_k and σ_ω are the turbulent Prandtl numbers for k and ω. Moreover, μ_t is the turbulent viscosity, which is written in (10) as,

$$\mu_t = \frac{\rho k}{\omega} \frac{1}{max\left[\frac{1}{\alpha^*}, \frac{SF_2}{\alpha_1 \omega}\right]}, \tag{10}$$

where, S represents the strain rate magnitude. σ_k is the turbulent Prandtl numbers for k and σ_ω is the turbulent Prandtl numbers for ω, and are calculated by Equations (11) and (12), respectively [37]:

$$\sigma_k = \frac{1}{\frac{F_1}{\sigma_{k,1}} + \frac{(1-F_1)}{\sigma_{k,2}}} \tag{11}$$

$$\sigma_\omega = \frac{1}{\frac{F_1}{\sigma_{\omega,1}} + \frac{(1-F_1)}{\sigma_{\omega,2}}} \tag{12}$$

In Equation (10) α^* dampens turbulent viscosity, leading to a low Reynolds number modification, which is given in (13) as follows,

$$\alpha^* = \alpha_\infty^* \left(\frac{0.024 + \frac{\rho k}{6\mu\omega}}{1 + \frac{\rho k}{6\mu\omega}} \right) \tag{13}$$

Moreover, F_1 and F_2 are the blending functions, which are given in Equations (14) and (15):

$$\begin{cases} F_1 = tanh\left\{ \left(min\left[max\left(\dfrac{\sqrt{k}}{0.09\omega y}, \dfrac{500\mu}{\rho y^2 \omega} \right), \dfrac{4\rho k}{\sigma_{\omega,2} D_\omega^+ y^2} \right] \right)^4 \right\} \\ D_\omega^+ = max\left[2\rho \dfrac{1}{\sigma_{\omega,2}} \dfrac{1}{\omega} \dfrac{\partial k}{\partial x_j} \dfrac{\partial \omega}{\partial x_j}, 10^{-10} \right] \end{cases} \tag{14}$$

$$F_2 = tanh\left\{ \left(max\left[2\frac{\sqrt{k}}{0.09\omega y}, \frac{500\mu}{\rho y^2 \omega} \right] \right)^2 \right\} \tag{15}$$

where the distance to the adjacent surface is denoted by y. It is worth noting that D_ω^+ represents the positive part of the cross-diffusion term, which is thoroughly discussed in Ref. [38].

3.3. Surface Dynamics of Wave

The wave motion of the sea surface should be considered in the modelling process. Among the several theories to account for the wave dynamics, in this study, the Airy wave theory, which is often referred to as linear wave theory, has been employed.

This theory describes the transmission of gravity waves on the surface of a uniform fluid layer in a linearized manner. The fluid layer has a homogeneous mean depth, and the fluid flow is irrotational, incompressible, and inviscid, according to the hypothesis. Ref. [39] contains more information on the Airy wave theory, which is not included here to save the page size.

4. Simulation Setup

A two-dimensional numerical domain is provided based on the results in [11, 40] to validate the model and compare the performance of the novel system to that of the conventional OWC system. For the conventional OWC system, the results reported by Elhanafi et al. [11] (which has the same dimension properties as the proposed hybrid system in this study) is employed. Air and water compressibility is considered negligible since the pressure required to compress the air density within the system is small. However, because air compressibility has the potential to influence system performance, it should be considered when analyzing full-scale systems [41]. The water's free surface, the chamber area for modelling air compression and decompression, and the windcatcher and its surroundings make up the three-part of the numerical domain.

As shown in Figure 5, the domain has a length of 4500 mm and a height of 27200 mm. The spacing between the boundaries is assumed to be large enough to prevent boundary conditions from hurting the results of probs inside the converter and other dimensions for inlet parameters like wind and wave. The domain exit is 12433 mm away from the backside lip of the system, while the front lip of the converter is 14596 mm away from the inlet boundary. Furthermore, in all analyses, the height of

the free surface area is assumed to be three times the wave height. The orifice that represents the converter's PTO has a diameter of 2.5mm.

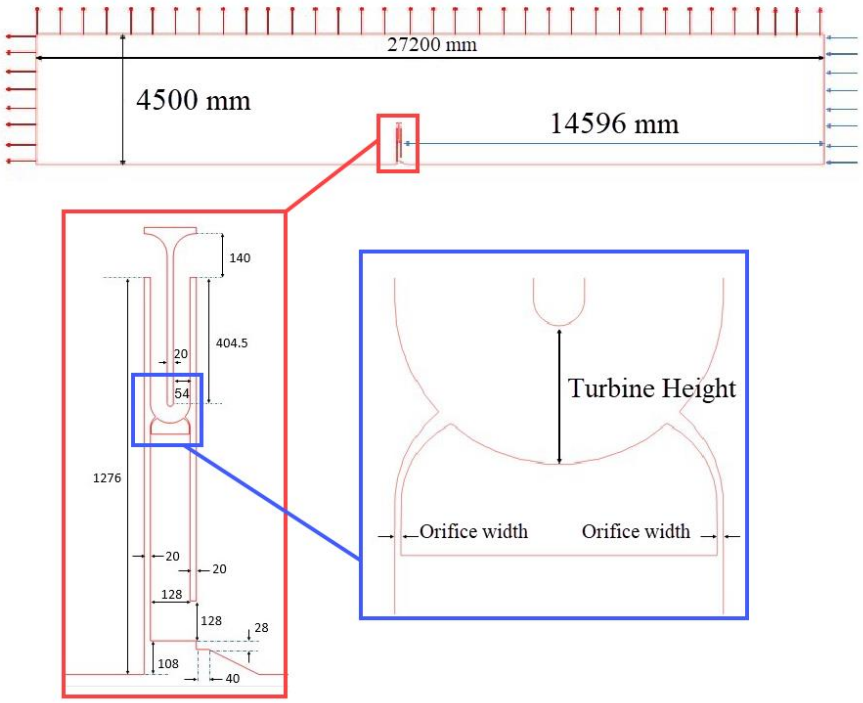

Figure 5. Schematic of the geometrical specifications and the computational domain.

The simulation is performed using the Ansys 19 R2 software package which uses the transient mode of modelling in two-dimensional form. An open channel flow with boundary conditions, as well as a tank developed for a broader range of wind and wave conditions, is used to model wave propagation. The calculations use a linear form of waves with 0.04 m wave heights, 1.4 s wave periods, and 0.42 m water depths, respectively. With an initial wind speed of 0.85 m/s added to the simulation, the inlet boundary is specified as velocity-inlet, and segregated velocity input is used to model the airflow within the domain. The outlet boundary is adjusted to the pressure outlet, and non-slip walls are used. To model the turbulent viscosity of incompressible air and water, the two-equation SST $k-\omega$ is used. The volume of fluid open channel flow and open channel wave boundary conditions with implicit volume fraction variables are included to model the wave fluctuations within the specified tank using the multiphase technique.

4.1. Mesh Independence Analysis

The mesh independence testing is used to show that a solution is unaffected by the geometry grid size. In the mesh independence analysis, four mesh sizes are evaluated: 185897 (grid #1), 421813 (grid #2), 745778 (grid #3), and 1772280 (grid #4). The airflow rate results for the left valve (LV) for simulations of the selected grid sizes are shown in Figure 6. The simulation results for the grids with 745778 and 1772280 total number of mesh elements are shown to be very similar. To ensure that the desired grid size is as accurate as possible, the maximum error of results for each grid size is calculated and summarized in Table 1. Grid #3 has an error of 3.29 % compared to grid #4 for the airflow rate results for the left valve, which is within the satisfactory margin. Therefore, in terms of computational cost, grid #3 is the better option. The airflow rate results for the right valve (RV) for simulations of the selected grid sizes are shown in Figure 7. The modelling findings of the grid with sizes of 745778 and 1772280 are shown to be in good agreement. The maximum error of results for each grid size has been calculated and listed in Table 1 to confirm that the intended grid size is accurate. As can be seen, grid #3 has a 3.51% error in the airflow rate results for the right valve when compared to grid #4. According to the obtained results of mesh analysis, grid #3 (i.e., grid with 745778 elements) achieves the maximum errors below 5% in all key performance indicators of the system, as thoroughly discussed in Table As a result, because the results are grid-independent, this grid will be used for the rest of the simulations. Besides, Figure 8 shows the employed mesh for the CFD model used in this study in more detail around the valves.

Table 1. Accuracy comparison of each chosen grid size versus the next grid size for the airflow rate results for the left valve (LV) and right valve (RV)

	Grid #1	**Grid #2**	**Grid #3**	**Grid #4**
Total number of mesh elements	185897	421813	745778	1772280
Maximum error compared to next grid size (%) for LV	9.97	6.53	3.29	-
Maximum error compared to next grid size (%) for RV	13.82	5.02	3.51	-

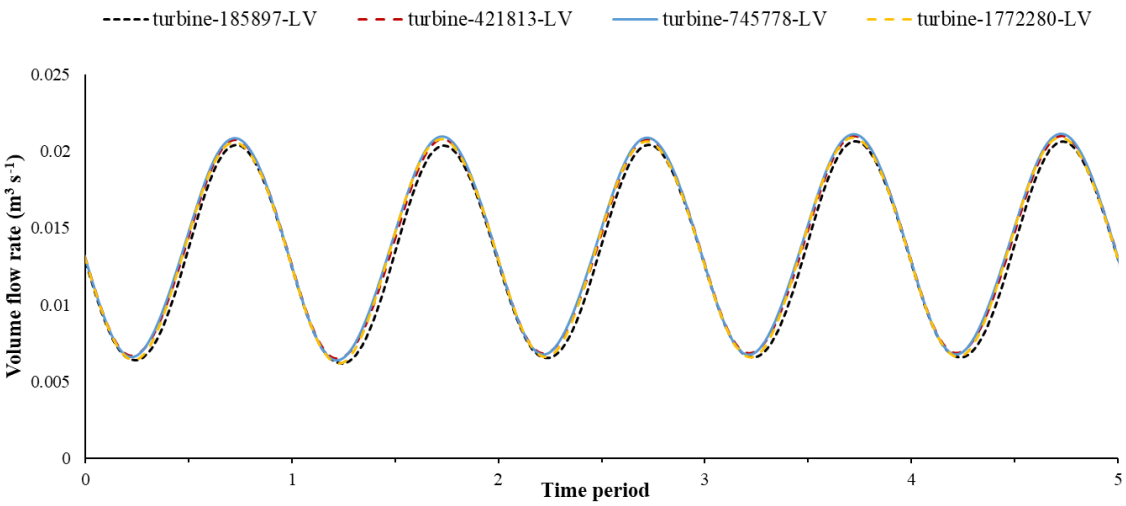

Figure 6. Airflow rate results for the left valve (LV) for four grid sizes with a total of 185897, 421813, 745778, and 1772280 mesh elements.

4.2 Time Step Independence Analysis

Grid independence is achieved in the previous section. Since this is a transient study, the chosen time step of the simulation should be examined to obtain accurate results. Five-time step settings of 0.0014s, 0.0007s, 0.00056s, 0.00035s, and 0.00028s are chosen and sensitivity analysis is performed with them.

The water elevation inside the chamber is shown in Figure 9 for the selected time steps. As can be seen, the results for time steps of 0.0014s and 0.0007s are exceedingly inaccurate. Moreover, the water level results for time steps of 0.00028s and 0.00035s are in good agreement and fluctuate between 0.39m and 0.45m approximately. Therefore, the results of Figure 9 indicate that a time step of 0.00035s is the best choice.

The results of the turbine flow rate are highlighted in Figure 4 for the specified time steps. The results for time steps of 0.0014s and 0.0007s are very unreliable, as can be seen. Moreover, the turbine flow rates vary between 0.009 $m^3 s^{-1}$ and 0.037 $m^3 s^{-1}$ at time steps of 0.00028s and 0.00035s, which are in perfect agreement. As a result, Figure 4 shows that a time step of 0.00035s is the best choice, which is consistent with the results of the water level inside the chamber presented in Figure 2. Moreover, the

simulation is performed on the system with AMD EPYC 7501 32-core 2GH processor and 32GB RAM. Figure 11 reports the simulation run time for different grids and time steps. Figure 10a shows the simulation run-time for time step of 0.007s in the smallest and largest grid sizes intended to perform grid independence analysis. Further, Figure 10b reports the simulation run-time for the grid size of 745,000 at different time steps. As seen, for the time step selected for the simulations (Dt = 0.00035s), the approximate run-time of each simulation was about 264 hours.

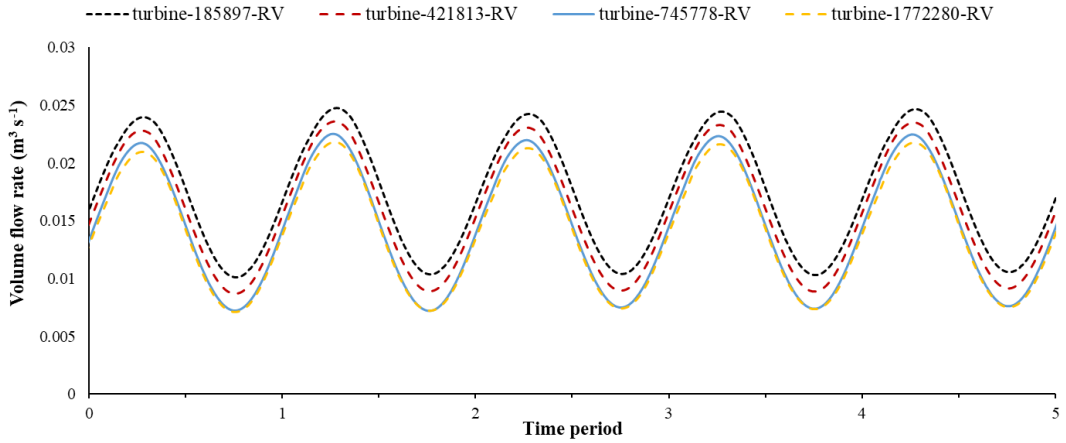

Figure 7. Airflow rate results for the right valve (RV) for four grid sizes with a total of 185897, 421813, 745778, and 1772280 mesh elements.

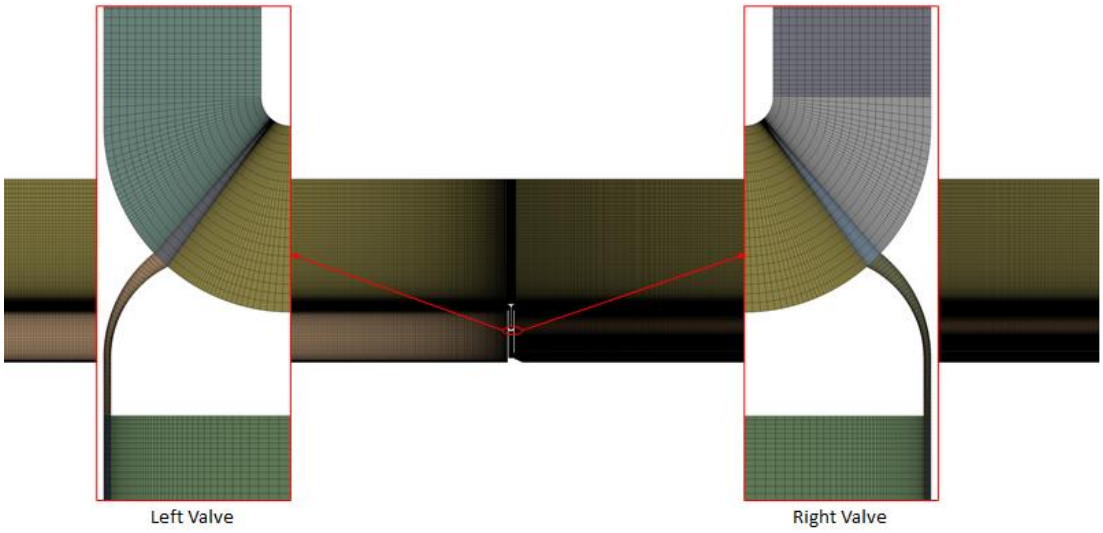

Figure 8. The employed mesh for the CFD mesh

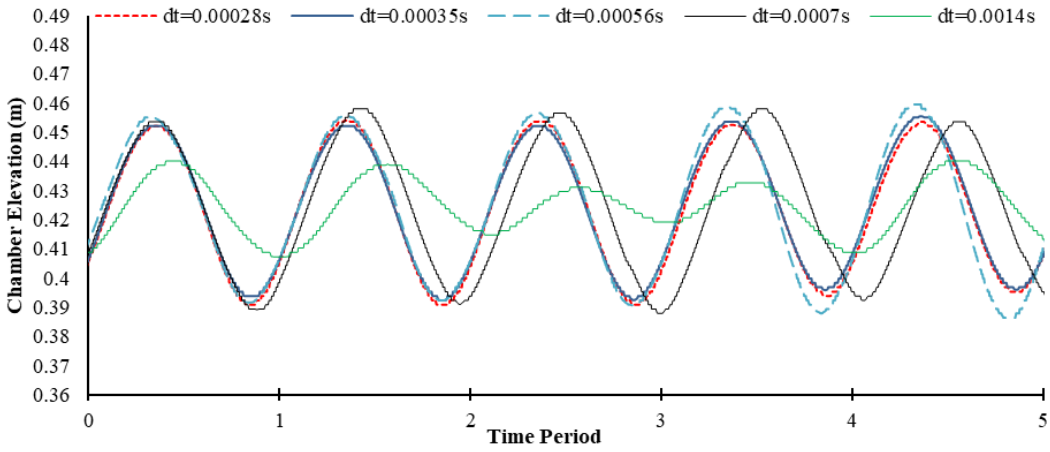

Figure 9. Water level within the chamber for five time steps of 0.0014s, 0.0007s, 0.00056s, 0.00035s, and 0.00028s.

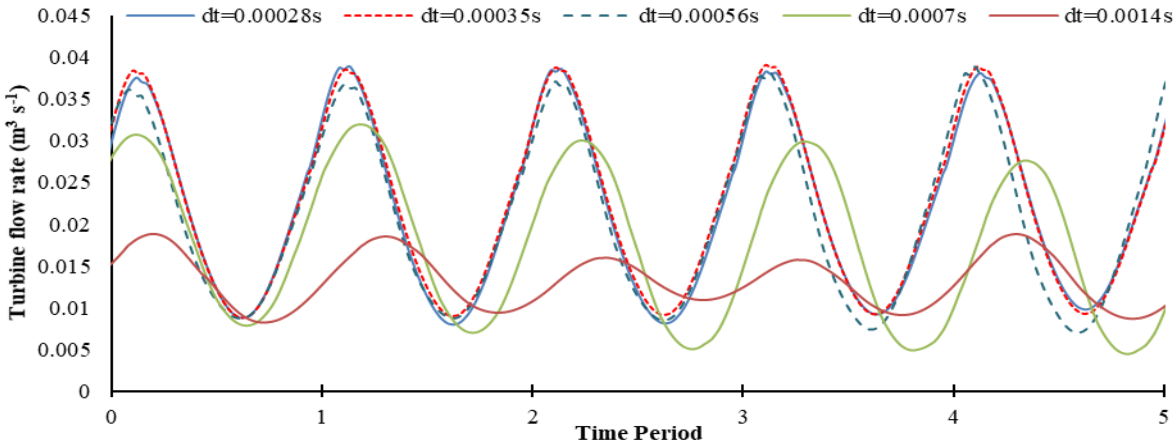

Figure 10. Results of turbine flow rate for five-time steps of 0.0014s, 0.0007s, 0.00056s, 0.00035s, and 0.00028s.

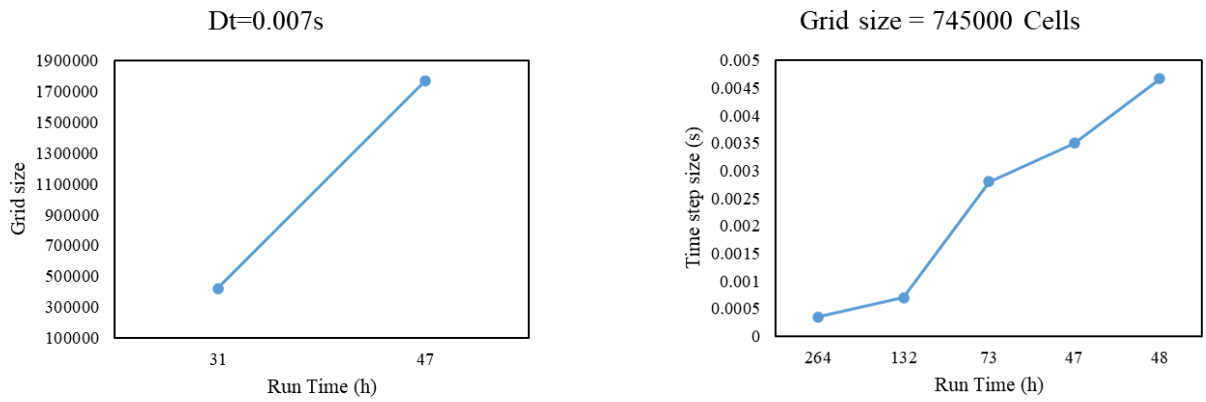

(a) (b)

Figure 11. Run time of simulation for different grids and time steps.

5. Results and Discussion

The numerical model that is used to examine the proposed hybrid wave-wind WEC is described in the earlier sections, and the model's sensitivity to grid and time step has been investigated. In this section, the results of the proposed numerical procedure are validated using experimental and numerical data. Then, to provide more in-depth knowledge of the findings, the performance of the proposed design is compared to the conventional system from different aspects. Wind flow does not affect the performance of conventional WEC (i.e., the system that used in Ref. [11] and shown in Figure 1) designs because they are not wind-affected. On the other hand, because of the significant energy of the wind flow, combining it with WEC can significantly improve power generation. Therefore, multiple wind speeds are simulated to further examine the proposed design. Important parameters to consider are output power, turbine flow rate, orifice, and windcatcher flow rate, water level, and pressure within the chamber.

Figure 12 compares the results of the conventional WEC model for wave height H = 40mm, periodicity T = 1.4s, water depth h = 420mm and orifice width e = 2.5mm with experimental [40] and numerical [11] data. Besides, wp1, wp2 and wp3 are three points at the x=15.3, x=15.6, and x=16m as defined in [11]. As seen, the simulation results of the present work are in good agreement with the experimental and numerical results.

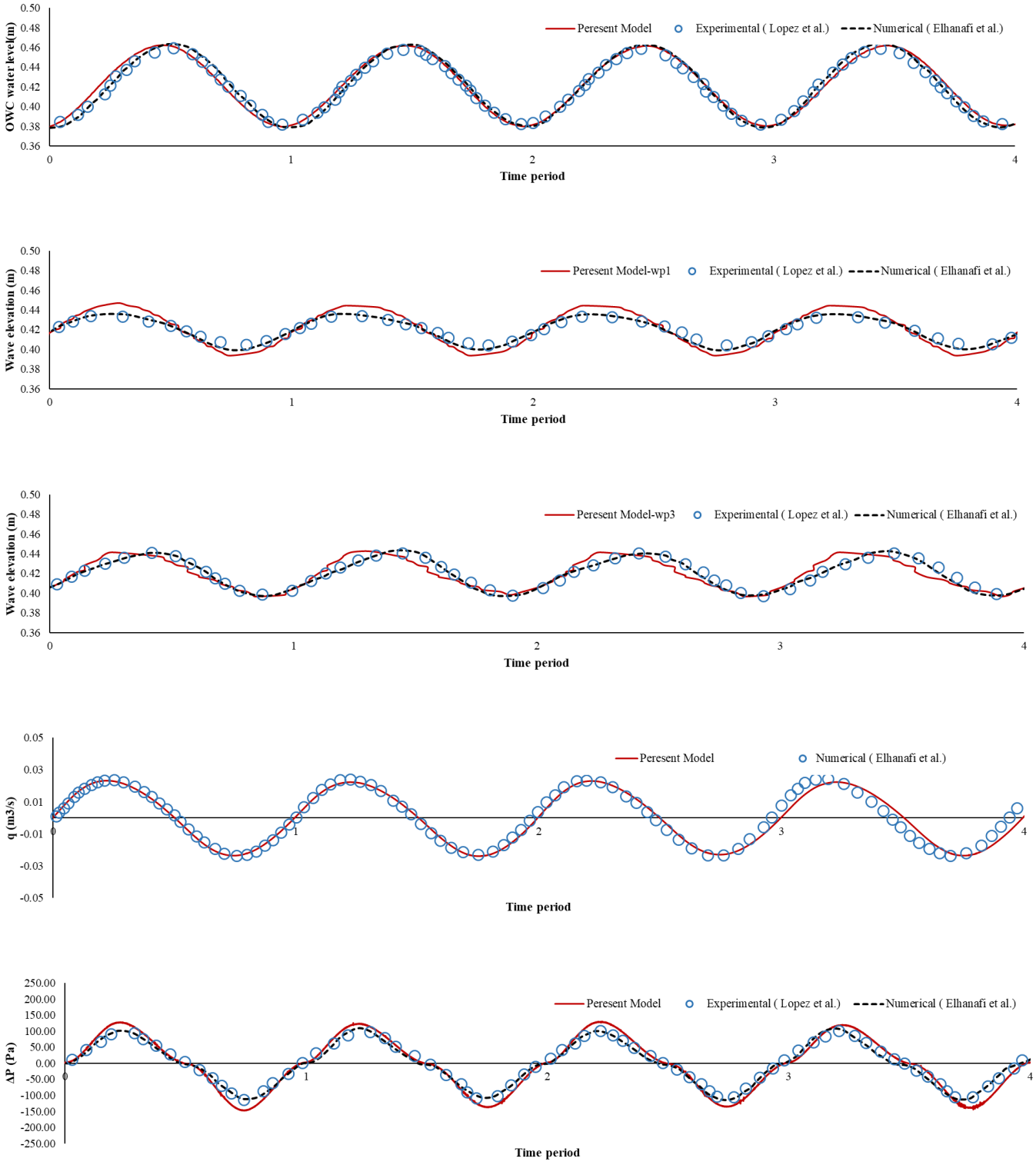

Figure 12. Comparison of simulation results with numerical [11] and experimental work [40]: From top to bottom: chamber water height, water level height in wp1 and wp3, flow rate passing through the orifice and pressure difference of the chamber inside and outside. The wp1, wp2 and wp3 are three points at the x=15.3, x=15.6, and x=16m as defined in[11]

As discussed earlier, the high level of wind flow in coastal regions inspires the use of wind energy in conventional WECs. Incorporating wind energy into the system and combining it with wave energy is the major contribution of the proposed design. Figure 13 represents the entrance wind flow rate to the windcatcher, the flow rate caused by the movement of the water level within the chamber, the simulated turbine flow rate, and the maximum turbine flow rate. The difference between the simulation result and the maximum turbine flow rate (sum of wind and wave flow) is because the geometry under consideration is not optimal. As a result, to achieve the maximum turbine flow, the geometry should be optimized and some geometric parameters, such as the orifice output angle, need to be modified.

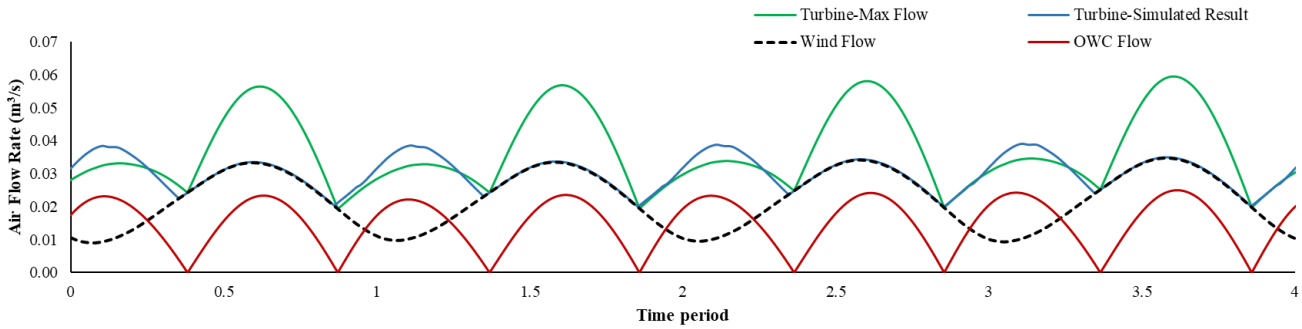

Figure 13. Distinction of wind flow, wave, simulated turbine flow, and maximum turbine flow.

The direction of flow on the turbine in a conventional OWC change with each period. As a result, a bidirectional turbine, such as a wells turbine, is required. The new system proposed in this paper is designed to eliminate airflow direction change. The turbine flow in the conventional OWC model and the hybrid wind-wave energy converter is presented in Figure 14. As shown, the combination of wind flow and wave flow that increases net flow through the turbine and the direction of flow through the turbine in both systems. The oscillation amplitude of the turbine flow is reduced from an average of 0.047 m^3 s^{-1} to 0.02 m^3 s^{-1} in the hybrid model. This decrease improves the uniformity of energy production.

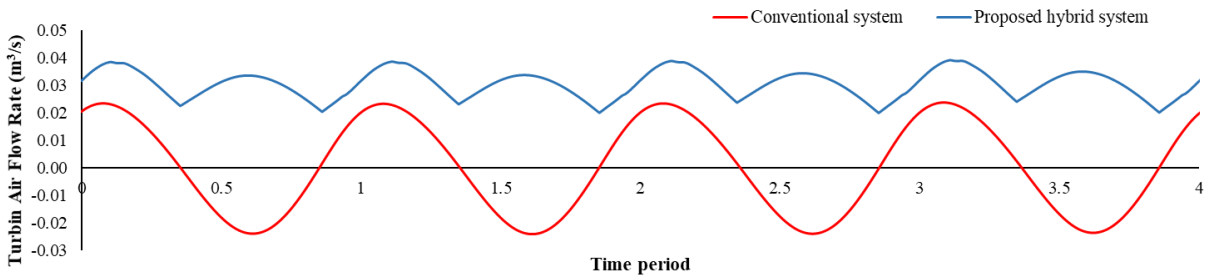

Figure 14. Turbine air flow rate in conventional model reported by Elhanafi et al. [11] and hybrid model proposed in this study.

Figure 15 represents the water level inside the chamber, the pressure difference between the inside and outside of the chamber, the airflow rate through the turbine, and the maximum power output in conventional and proposed hybrid models. The amount of output energy in the hybrid wind-wave system increases as wind energy enters the system. As can be seen, the turbine always has a considerable amount of airflow, indicating that even when the wave causes no airflow, the wind captured by the windcatcher provides the airflow rate and the system's output power is not zero. Besides, the maximum output power of conventional wind turbines is calculated using this equation: $P = 0.5.r.A.V^3$. Figure 15 illustrates this attribute. It can be concluded that, in the proposed system, due to the unidirectional flow through the turbine, a variety of turbines that perform better than wells turbines can be used.

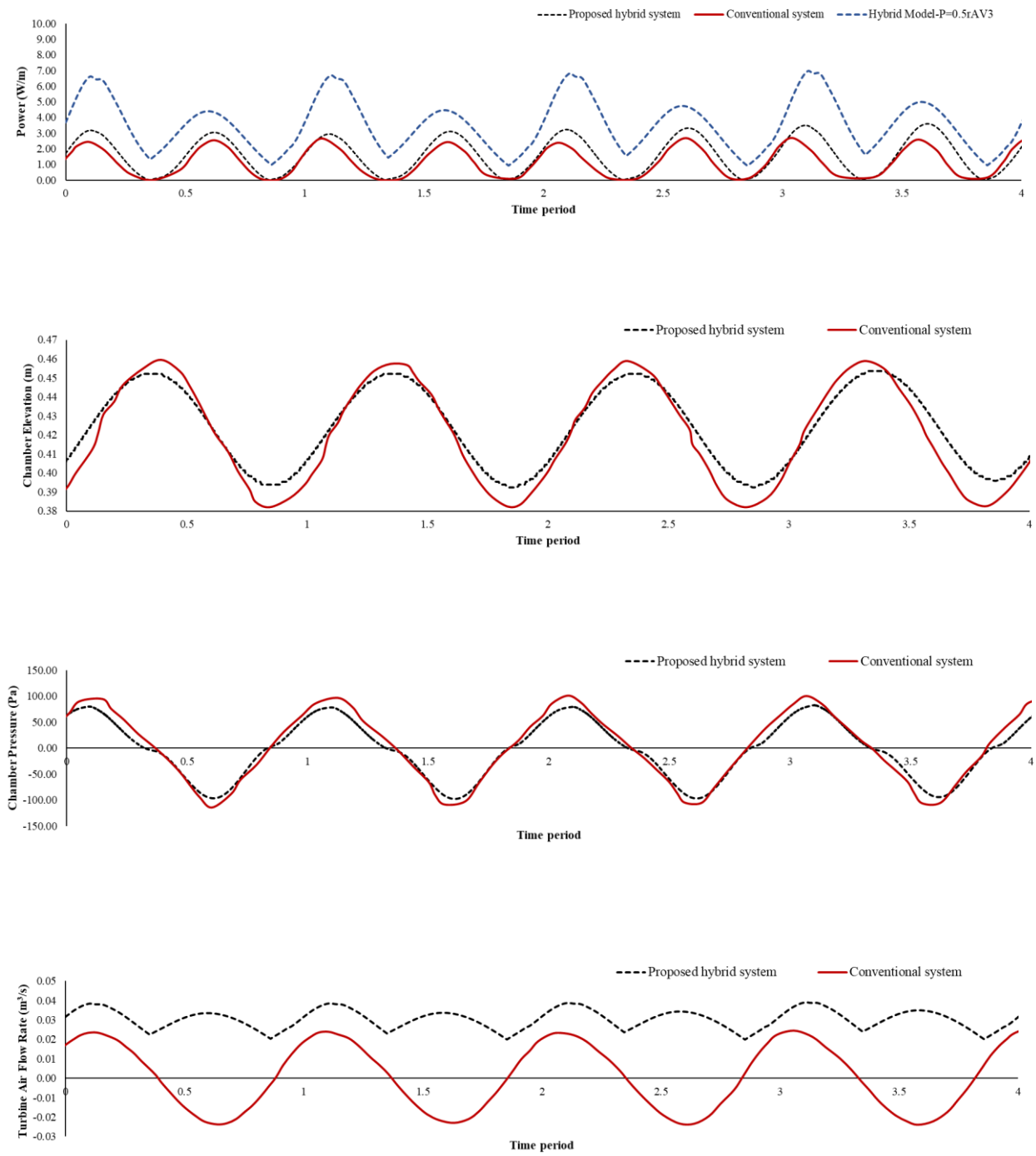

Figure 15. Comparison of hybrid model results with the conventional model. Top-down: chamber water level, inside and outside chamber pressure difference and flow rate through Orifice.

The effect of wind speed on the performance of the proposed design at three different wind speeds of 0.7, 0.85, and 1 m/s is investigated. It is worth mentioning that the selected wind speeds have been selected based on the variable scaling using the Froude concept, which is thoroughly provided by

López et al. [40]. The flow rate of air entering the windcatcher increases as the wind speed increases. The average amount of turbine airflow rate increases while the airflow rate profile remains unchanged. Increasing the airflow rate increases the speed of the turbine blades and consequently its output power. As a result, wind speed is a critical factor in this system. It's worth noting that the airflow provided by the wave is unaffected by wind speed. The effect of changing the wind speed on the inlet flow to the windcatcher is shown in Figure 16. The results show that changing the wind speed from 0.85m/s to 1m/s has a greater effect than changing the speed from 0.7m/s to 0.85m/s. Moreover, Figure 17 shows the percentage change in entrance flow to the windcatcher due to changes in wind speed. As shown, changing the speed from 0.7m/s to 0.85m/s and 0.85m/s to 1m/s results in an average increase of 12.3% and 26.9% in the inlet flow rate to the windcatcher, respectively. While the maximum increase is approximately 60%.

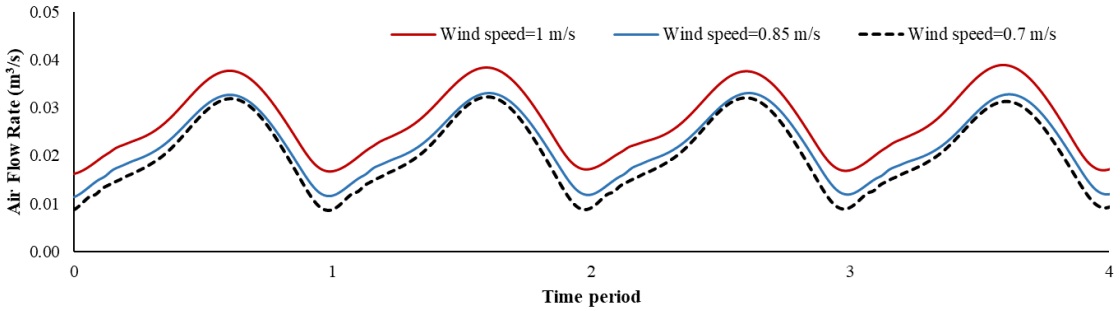

Figure 16. The effect of wind speed on entrance flow to the windcatcher.

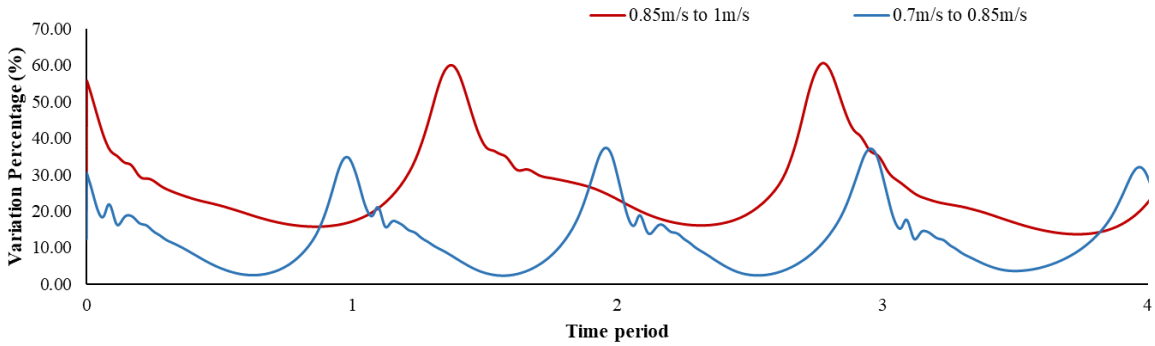

Figure 17. Variation percentage in entrance flow to windcatcher due to change in wind speed.

Figure 18 shows the turbine airflow rate at different wind speeds. As shown, throughout the entire period of the conducted simulation, the passing airflow rate through the turbine wouldn't be zero. The

results confirm that the minimum airflow rate of the turbine is around 50%, 48%, and 45% of its maximum airflow rate for wind speeds of 1 m/s, 0.85 m/s, and 0.7 m/s, respectively. The effects of this continuous air flow rate on power generation are shown in Figure 19. As shown, the proposed hybrid system achieves continuous power generation during its operation. Furthermore, the speed of wind has a significant effect on the produced power, emphasizing the crucial role of incorporating a windcatcher into the system. According to the obtained results, adjusting the orifice angle of the proposed hybrid design results in more uniform output power.

As previously stated, the wind has no effect on the wave's output power generation in OWC systems. Figure 20 represents the velocity and fluid fraction contours at two wind speeds of 0.7m/s and 1m/s to demonstrate this claim. The wind does not affect the height of the water level inside the chamber, as can be seen. As a result, changing the wind speed has no effect on the water velocity distribution or the water height in the chamber. In addition, the inlet and outlet airflow from the chamber remain unchanged, in contrast to the new design introduced in this paper, which benefits the wind and waves energy to generate power.

Figure 21 depicts the combined effect of velocity fields produced by the airflow rate of wave motion in the chamber and the airflow rate provided by the windcatcher. This reflects several flow characteristics to develop, such as a strong vortex at the bottom lip and weaker vortices at the upper lip and entry into the chamber. These vortices are formed by a sudden change in geometry and the interaction of two different airflows, which causes the flow to separate and also gradually dissipates energy from the vortex's core. The transient simulation shown in Figure 21 confirms that vortex generation decreases with time; however, vortex formation should be reduced through geometry optimization.

The following items are suggested for future research path to acquire a thorough understanding of the topic: (1) geometric modifications and optimizations of the primary design of the hybrid wave-wind wave energy converter introduced in this paper, including orifice output angle,

turbine height, windcatcher inlet diameter, the distance between the air inlet and outlet valves, windcatcher inlet height of the turbine, windcatcher width size, and overall windcatcher geometry, (2) examine the wave characteristics and wind speed profiles. (3) In this study, the orifice output angle is configured so that high-speed airflow is directed to the turbine. However, a part of the exhaust airflow may not pass through the turbine, which is undesirable. The proportion of airflow that enters the turbine is determined by the geometric design, particularly the orifice output angle and windcatcher geometrical design. Consequently, an optimization study to account for the amount of exhaust airflow rate that enters the turbine is beneficial. However, it is outside the scope of this paper.

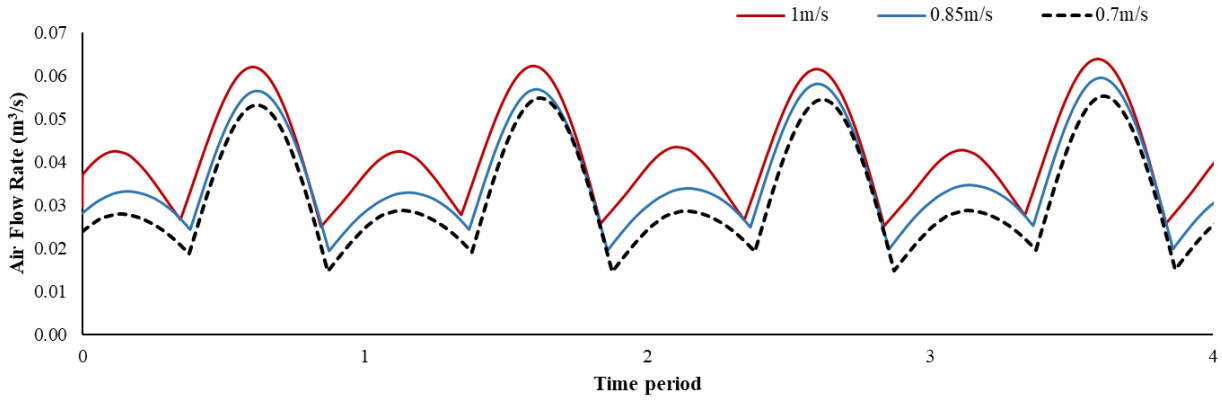

Figure 18. The variation of the turbine flow at different wind speeds.

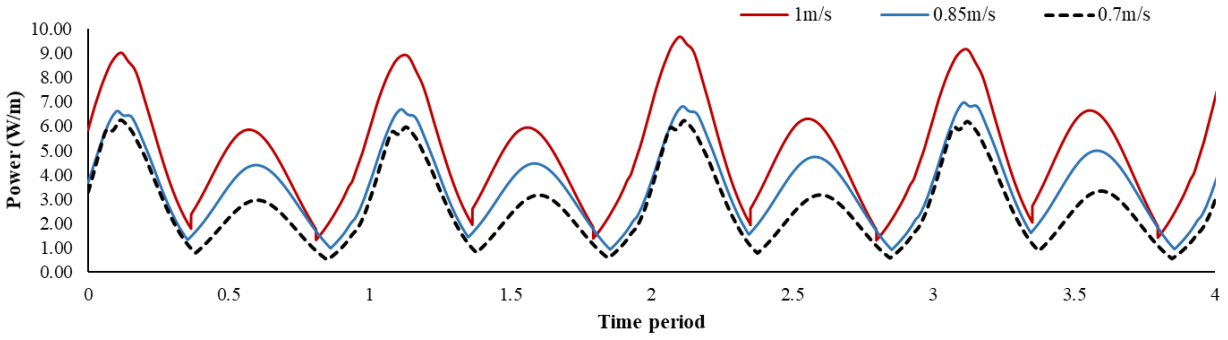

Figure 19. The variation of the output power at different wind speeds.

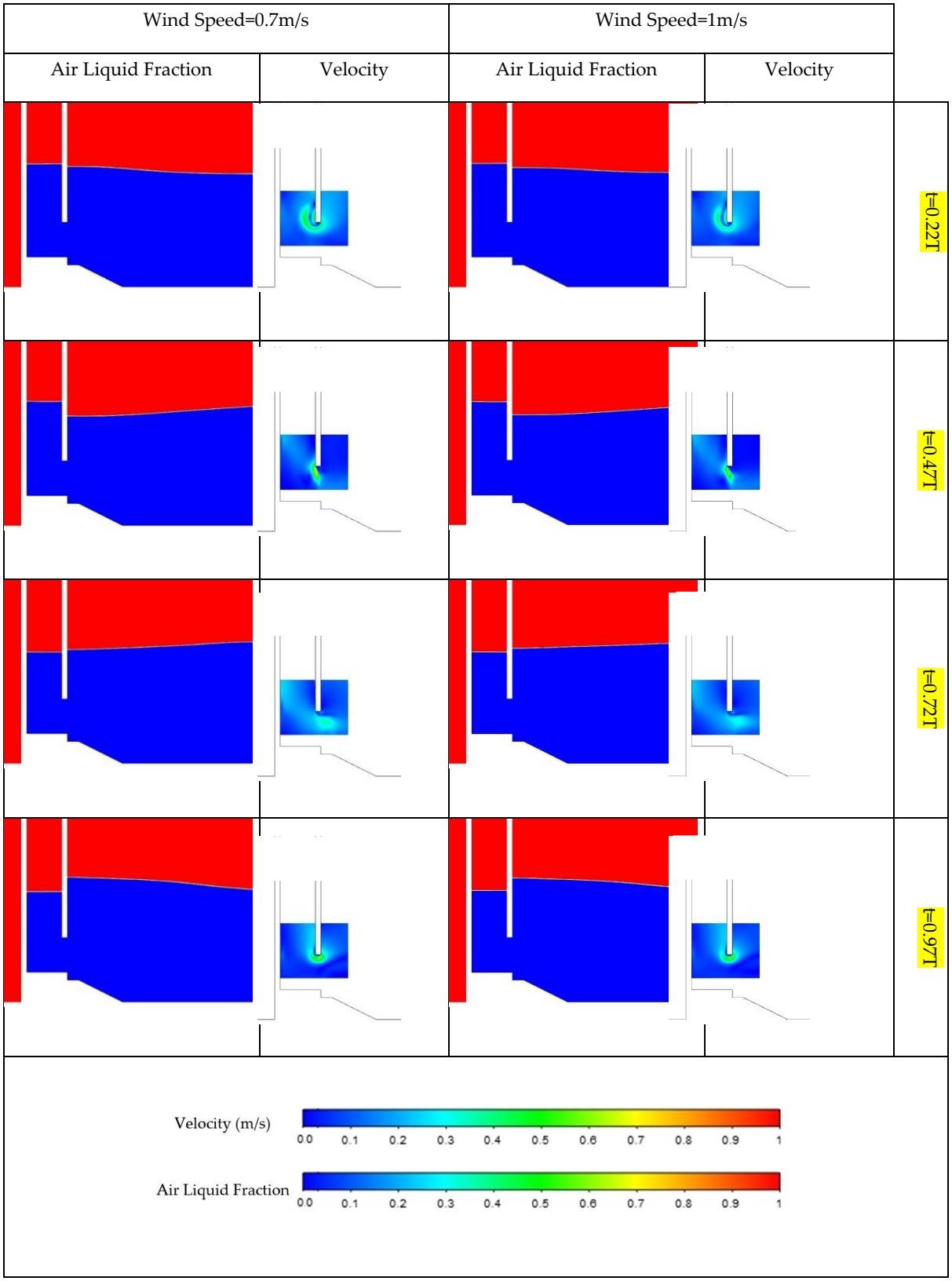

Figure 20. Liquid fraction and velocity Contours of two different wind speed at different times.

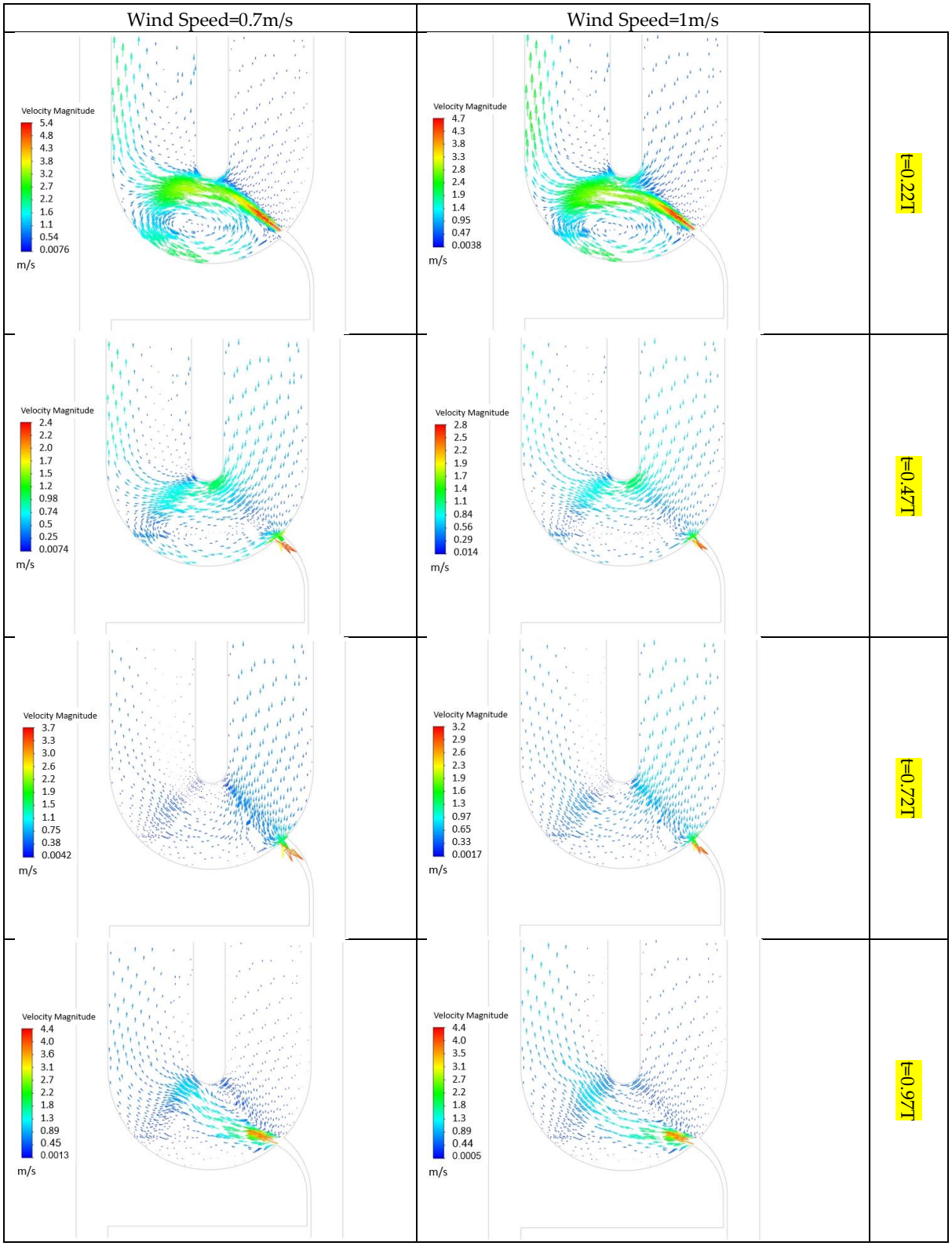

Figure 21. Transient behaviour of the airflow velocity field is caused by a combination of the airflow rate of wave motion in the chamber and the airflow rate provided by the windcatcher for different wind speeds.

6. Conclusions

A novel OWC WEC incorporated with wind energy is investigated. The potential of combining wave and wind energy by a windcatcher to increase airflow rate through turbine blades has been studied. In addition to wind energy, two one-way valves are used to control airflow in this novel design. As a result, the airflow always enters the turbine in the same direction. The CFD approach based on the RANS technique is used to simulate this new design, and the results are compared to a conventional OWC model. Besides, the shear-stress transport (SST) $k-\omega$ model has been used to account for the turbulent behaviour of the flow. The model has been validated for OWC chamber water height, water level elevation, flow rate passing through the orifice and pressure difference of the chamber using previous experimental and numerical studies. Consequently, the verified model has been used to simulate the proposed model from various operational perspectives, using space and time-independent grids.

The main contribution of this study is the use of windcatchers to harness wind energy in conjunction with the OWC wave energy converter to generate power in coastal regions. Another novel aspect of this research is the conversion of bidirectional flow through the turbine to unidirectional flow, which enables the use of turbines with higher efficiency and continuous output power. It is found that the turbine always has a considerable fraction of airflow, highlighting the significance of incorporating the windcatcher into the proposed hybrid system, which provides the airflow rate even when no airflow is generated by the wave, and the system's output power is not zero. The results showed that combining wind flow and wave flow enhances the overall airflow rate through the turbine as well as the direction of flow through the turbine in both systems. In the proposed hybrid system, the oscillation amplitude of the turbine airflow rate is diminished from an average of 0.047 $m^3\ s^{-1}$ to 0.02 $m^3\ s^{-1}$. This reduction realises power generation consistency.

Because the given airflow rate by the windcatcher, and consequently the produced power, is heavily influenced by wind speed, the effect of wind speed on the performance of the proposed hybrid

model is evaluated at three distinct wind speeds of 0.7, 0.85, and 1 m/s. According to the results, boosting the wind speed by 0.85m/s caused a more serious impact than raising it by 0.7 m/s. Furthermore, increasing the wind speed from 0.7 m/s to 0.85 m/s and 0.85 m/s to 1 m/s led to an improvement in the intake flow rate to the windcatcher of 12.3 % and 26.9 %, correspondingly. While the highest possible increase is roughly 60 %. This study's findings verified that the proposed hybrid wave-wind OWC can outperform the conventional OWCs in terms of power generation and functionality; nevertheless, further geometry optimization can be made to improve the system performance.

References

[1] S. Doyle and G. A. Aggidis, "Development of multi-oscillating water columns as wave energy converters," *Renewable and Sustainable Energy Reviews,* vol. 107, pp. 75-86, 2019.

[2] D. Qiao, R. Haider, J. Yan, D. Ning, and B. Li, "Review of Wave Energy Converter and Design of Mooring System," *Sustainability,* vol. 12, no. 19, p. 8251, 2020.

[3] B. Kamranzad and S. Hadadpour, "A multi-criteria approach for selection of wave energy converter/location," *Energy,* vol. 204, p. 117924, 2020.

[4] A. F. Falcão and J. C. Henriques, "The spring-like air compressibility effect in oscillating-water-column wave energy converters: Review and analyses," *Renewable and Sustainable Energy Reviews,* vol. 112, pp. 483-498, 2019.

[5] F. d. O. Antonio, "Wave energy utilization: A review of the technologies," *Renewable and sustainable energy reviews,* vol. 14, no. 3, pp. 899-918, 2010.

[6] T. Heath, "A review of oscillating water columns," *Philosophical Transactions of the Royal Society A: Mathematical, Physical and Engineering Sciences,* vol. 370, no. 1959, pp. 235-245, 2012.

[7] A. F. Falcão and J. C. Henriques, "Oscillating-water-column wave energy converters and air turbines: A review," *Renewable Energy,* vol. 85, pp. 1391-1424, 2016.

[8] N. Delmonte, D. Barater, F. Giuliani, P. Cova, and G. Buticchi, "Review of oscillating water column converters," *IEEE Transactions on Industry Applications,* vol. 52, no. 2, pp. 1698-1710, 2015.

[9] Y. Sang, H. B. Karayaka, Y. Yan, N. Yilmaz, and D. Souders, "1.18 ocean (marine) energy," 2018.

[10] A. F. Falcão, J. C. Henriques, and L. M. Gato, "Self-rectifying air turbines for wave energy conversion: A comparative analysis," *Renewable and Sustainable Energy Reviews,* vol. 91, pp. 1231-1241, 2018.

[11] A. Elhanafi, A. Fleming, G. Macfarlane, and Z. Leong, "Numerical energy balance analysis for an onshore oscillating water column–wave energy converter," *Energy,* vol. 116, pp. 539-557, 2016.

[12] W. Chen and W. Liu, "Numerical simulation of the airflow and temperature distribution in a lean-to greenhouse," *Renewable energy,* vol. 31, no. 4, pp. 517-535, 2006.

[13] D. D. Raj, V. Sundar, and S. Sannasiraj, "Enhancement of hydrodynamic performance of an Oscillating Water Column with harbour walls," *Renewable Energy,* vol. 132, pp. 142-156, 2019.

[14] G. Malara, A. Romolo, V. Fiamma, and F. Arena, "On the modelling of water column oscillations in U-OWC energy harvesters," *Renewable Energy,* vol. 101, pp. 964-972, 2017.

[15] K. Rezanejad and C. G. Soares, "Enhancing the primary efficiency of an oscillating water column wave energy converter based on a dual-mass system analogy," *Renewable Energy,* vol. 123, pp. 730-747, 2018.

[16] A. Moñino, E. Medina-López, R. J. Bergillos, M. Clavero, A. Borthwick, and M. Ortega-Sánchez, "Effects of Seabed Morphology on Oscillating Water Column Wave Energy Converter Performance," in *Thermodynamics and Morphodynamics in Wave Energy*: Springer, 2018, pp. 67-85.

[17] D. Ning, Y. Zhou, and C. Zhang, "Hydrodynamic modeling of a novel dual-chamber OWC wave energy converter," *Applied Ocean Research,* vol. 78, pp. 180-191, 2018.

[18] A. Elhanafi, A. Fleming, G. Macfarlane, and Z. Leong, "Underwater geometrical impact on the hydrodynamic performance of an offshore oscillating water column–wave energy converter," *Renewable Energy,* vol. 105, pp. 209-231, 2017.

[19] C. Xu and Z. Huang, "Three-dimensional CFD simulation of a circular OWC with a nonlinear power-takeoff: Model validation and a discussion on resonant sloshing inside the pneumatic chamber," *Ocean Engineering,* vol. 176, pp. 184-198, 2019.

[20] B. Goeijenbier, J. Bricker, A. Antonini, G. Malara, M. Hendriks, and H. van der Ham, "Structural Optimisation and Behaviour of the Breakwater Integrated Oscillating Water Column Device: A combined 3D CFD and Structural FEM Analysis," *Journal of Coastal and Hydraulic Structures,* vol. 1, 2021.

[21] E. Saedpanah and H. Pasdarshahri, "Performance Assessment of Hybrid Desiccant Air Conditioning Systems: a Dynamic Approach Towards Achieving Optimum 3E Solution Across the Lifespan," *Energy,* p. 121151, 2021.

[22] O. Saadatian, L. C. Haw, K. Sopian, and M. Y. Sulaiman, "Review of windcatcher technologies," *Renewable and Sustainable Energy Reviews,* vol. 16, no. 3, pp. 1477-1495, 2012.

[23] R. M. Kassir, "Passive downdraught evaporative cooling wind-towers: A case study using simulation with field-corroborated results," *Building Services Engineering Research and Technology,* vol. 37, no. 1, pp. 103-120, 2016.

[24] W. Sheng, T. Lewis, and R. Alcorn, "On wave energy extraction of oscillating water column device," in *Proceedings of the Fourth International Conference on Ocean Energy (ICOE), Dublin, Ireland*, 2012, pp. 17-19.

[25] P. R. Teixeira, R. A. Gonçalves, and E. Didier, "A RANS-VoF Numerical Model to Analyze the Output Power of An OWC-WEC Equipped with Wells and Impulse Turbines in A Hypothetical Sea-State," *China Ocean Engineering,* vol. 34, no. 6, pp. 760-771, 2020.

[26] M. Stovall *et al.*, "Dose to the contralateral breast from radiotherapy and risk of second primary breast cancer in the WECARE study," *International Journal of Radiation Oncology* Biology* Physics,* vol. 72, no. 4, pp. 1021-1030, 2008.

[27] C. K. Batchelor and G. Batchelor, *An introduction to fluid dynamics*. Cambridge university press, 2000.

[28] D. Howe, J.-R. Nader, and G. MacFarlance, "Experimental analysis into the effects of air compressibility in OWC model testing," *AWTEC 2018 Proceedings,* p. 449, 2018.

[29] W. Sheng and T. Lewis, "Energy conversion: A comparison of fix-and self-referenced wave energy converters," *Energies,* vol. 9, no. 12, p. 1056, 2016.

[30] I. Simonetti and L. Cappietti, "The impact of modelling air compressibility in the selection of optimal OWC design parameters in site specific wave conditions," in *International Conference on Offshore Mechanics and Arctic Engineering*, 2019, vol. 58899: American Society of Mechanical Engineers, p. V010T09A041.

[31] I. López, R. Carballo, F. Taveira-Pinto, and G. Iglesias, "Sensitivity of OWC performance to air compressibility," *Renewable Energy,* vol. 145, pp. 1334-1347, 2020.

[32] V. I. Terekhov, "Heat transfer in Highly Turbulent Separated Flows: A Review," *Energies,* vol. 14, no. 4, p. 1005, 2021.

[33] M. García-Díaz, B. Pereiras, C. Miguel-González, L. Rodríguez, and J. Fernández-Oro, "CFD analysis of the performance of a double decker turbine for wave energy conversion," *Energies,* vol. 14, no. 4, p. 949, 2021.

[34] J. J. Aguilar-Fuertes, F. Noguero-Rodríguez, J. C. Jaen-Ruiz, L. M. García-Raffi, and S. Hoyas, "Tracking Turbulent Coherent Structures by Means of Neural Networks," *Energies,* vol. 14, no. 4, p. 984, 2021.

[35] F. R. Menter, "Two-equation eddy-viscosity turbulence models for engineering applications," *AIAA journal,* vol. 32, no. 8, pp. 1598-1605, 1994.

[36] A. Hellsten, "Some improvements in Menter's k-omega SST turbulence model," in *29th AIAA, Fluid Dynamics Conference*, 1998, p. 2554.

[37] P. Hu, Y. Li, C. Cai, H. Liao, and G. Xu, "Numerical simulation of the neutral equilibrium atmospheric boundary layer using the SST k-omega turbulence model," *Wind and Structures,* vol. 17, no. 1, pp. 87-105, 2013.

[38] T. P. Dhakal and D. K. Walters, "Curvature and rotation sensitive variants of the K-Omega SST turbulence model," in *Fluids Engineering Division Summer Meeting*, 2009, vol. 43727, pp. 2221-2229.

[39] J. Le Roux, "An extension of the Airy theory for linear waves into shallow water," *Coastal Engineering,* vol. 55, no. 4, pp. 295-301, 2008.

[40] I. López, B. Pereiras, F. Castro, and G. Iglesias, "Performance of OWC wave energy converters: influence of turbine damping and tidal variability," *International Journal of Energy Research,* vol. 39, no. 4, pp. 472-483, 2015.

[41] A. J. Sarmento and A. d. O. Falcão, "Wave generation by an oscillating surface-pressure and its application in wave-energy extraction," *Journal of Fluid Mechanics,* vol. 150, pp. 467-485, 1985.